Published in final edited form as:
Dev Biol. 2013 February 1; 374(1): 1–11. doi:10.1016/j.ydbio.2012.11.035.

A novel FoxD3 gene trap line reveals neural crest precursor movement and a role for FoxD3 in their specification

Tatiana Hochgreb-Hägele and **Marianne E. Bronner**
Division of Biology, California Institute of Technology, Pasadena, CA 91125, USA

Abstract

Neural crest cells migrate extensively and contribute to diverse derivatives, including the craniofacial skeleton, peripheral neurons and glia, and pigment cells. Although several transgenic lines label neural crest subpopulations, few are suited for studying early events in neural crest development. Here, we present a zebrafish gene/protein trap line *gt(foxd3-citrine)*^{ct110a} that expresses a Citrine fusion protein with FoxD3, a transcription factor expressed in premigratory and migrating neural crest cells. In this novel line, *citrine* expression exactly parallels endogenous *foxd3* expression. High-resolution time-lapse imaging reveals the dynamic phases of precursor and migratory neural crest cell movements from the neural keel stage to times of active cell migration. In addition, Cre-recombination produces a variant line FoxD3-mCherry-pA whose homozygosis generates a FoxD3 mutant. Taking advantage of the endogenously regulated expression of FoxD3-mCherry fusion protein, we directly assess early effects of FoxD3 loss-of-function on specification and morphogenesis of dorsal root ganglia, craniofacial skeleton and melanophores. These novel lines provide new insights and useful new tools for studying specification, migration and differentiation of neural crest cells.

Keywords

FoxD3; neural crest; zebrafish; live imaging; mutant

INTRODUCTION

The neural crest is a multipotent stem/progenitor cell population that is induced during gastrulation, at the border between neural and non-neural ectoderm (Basch et al., 2006). In mouse and chick embryos, neural folds elevate to form the neural tube. In zebrafish, however, secondary neurulation occurs in which the neural plate is reorganized by convergent extension into a neural keel, and subsequently into a neural rod. Orchestrated changes in cell polarity and cell adhesion then result in cavitation of the zebrafish neural tube. Common to all vertebrates, premigratory neural crest precursors reside within the dorsal aspect of the neural tube, from which they delaminate to migrate extensively along stereotypical pathways. Finally, they settle in sometimes very distant locations in the embryo and differentiate into diverse cell types, including cartilage and bone of the

Corresponding authors: Tatiana Hochgreb: hochgreb@caltech.edu. Marianne E. Bronner: mebronner@caltech.edu. *Contact information:* Division of Biology, California Institute of Technology. 1200 E. California Blvd., MC139-74, Pasadena, CA 91125, USA., Telephone: (+1) 626-395-3355, Fax: (+1) 626-449-8599.

craniofacial skeleton, neurons and glia of the peripheral nervous system, pigment cells, neuroendocrine cells, and smooth muscle cells of the cardiac outflow tract (Knecht and Bronner-Fraser, 2002; Le Douarin and Kalcheim, 1999).

The neural plate border is defined by the overlapping expression of border specifiers like Msx, Pax3/7 and Zic family members (Bang et al., 1999; Monsoro-Burq et al., 2005; Phillips et al., 2006; Sato et al., 2005). Newly induced premigratory neural crest precursors subsequently are characterized by expression of neural crest specifiers such as FoxD3, SoxE and Snail, that not only represent early presumptive neural crest markers, but also play important later roles in cell fate acquisition (Sauka-Spengler and Bronner-Fraser, 2008). FoxD3, a member of the forkhead/winged helix family of transcription factors, was originally characterized by expression in embryonic stem cells, embryonal carcinomas and neural crest cells (Clevidence et al., 1993; Labosky and Kaestner, 1998; Sutton et al., 1996). In the neural crest lineage, FoxD3 functions as a transcriptional repressor important for differentiation of neurons and glia, and its loss biases derivatives toward a mesenchymal fate (Teng et al., 2008). However, the early role of FoxD3 in neural crest specification remains uncharacterized.

In a gene/protein trap screen, we have isolated a zebrafish line utilizing the endogenous FoxD3 locus to drive expression of a FoxD3-Citrine fusion protein in premigratory and migrating neural crest cells. In this novel line, we find that *citrine* expression recapitulates endogenous *foxd3* expression, from initial neural crest induction, through emigration from the neural keel, and migration to the periphery. We use this line to analyze dynamic aspects of early neural crest development. In addition, we obtain a variant line FoxD3-mCherry-pA whose homozygosis produces a FoxD3 mutant that is highly likely to be a null. The results demonstrate roles for FoxD3 during early neural crest formation and development of melanophores. This novel line represents a valuable tool for studying early events in neural crest specification and migration.

MATERIALS AND METHODS

Animals

Adult fish and embryos were maintained as described (Westerfield, 1995). We used the transgenic line *Tg(foxd3:GFP)* (Gilmour et al., 2002)..

Identification of *ct110a* and Cre recombination

The *ct110a* line was isolated from a gene/protein trap screen as previously described (Trinh et al., 2011). To generate the *Gt(foxd3-mcherry)*^{ct110R} line, *Gt(foxd3-citrine)*^{ct110a} embryos were injected with 90 pg of *cerulean-cre* mRNA at the one-cell stage for germline recombination. The injected F_0 embryos were raised and crossed to wild type fish and F_1 embryos were sorted based on mCherry expression.

Determination of genomic integration

To determine the genomic integration site of the FlipTrap construct, we performed splinkerette-PCR as previously described (Trinh et al., 2011; Uren et al., 2009). Briefly, genomic DNA obtained from *Gt(foxd3-citrine)*^{ct110a} embryos was digested with AluI or HaeIII and subsequently ligated with annealed splinkerette adaptors (Spl-blunt: ccttggctcgtttttttttgcaaaaa and Spl-top: CGAATCGTAACCGTTCGTA-CGAGAATTCGTACGAGAATCGCTGTCCTCTCCAACGAGCCAG). To amplify the junctions between the genome and the Tol2 insertion, a nested PCR was performed on the ligated DNA using specific primers to amplify the 5′ and 3′ ends of the FlipTrap insertion (Trinh et al., 2011).

RACE PCR

5′ and 3′ RACE PCR libraries were synthesized using GeneRacer kit (Invitrogen). Total RNA was extracted from *Gt(foxd3-citrine)*^{ct110a} embryos using RNAqueous kit (Ambion). PCR amplification of 5′ and 3′ ends was performed using *citrine* gene-specific primers: Citrine_GSP_F: TACAAGACCCGC GCCG AGGTGAAGT, Citrine_GSP_nested_F: CTGGTGAACCGCATCGAGCTGAAGG, and Citrine_GSP_R: GTGATCGCGCTTCTCGTTGGGGTCT, Citrine_GSP_nested_R: GCCGATGGGGGTGTTCTGCTGGTAG, respectively. PCR products were purified in agarose gel and cloned in pCRII-TOPO vectors for sequencing.

In situ hybridization and Immunohistochemistry

Whole mount *in situ* hybridization was performed as described (Thisse et al., 1993) using probes for *foxd3* (Odenthal and Nusslein-Volhard, 1998), *citrine* and *mcherry.* For *citrine* and *mcherry* probes, the full-length sequence was PCR amplified (primers: SP6_citrine_F:

GATTTAGGTGACACTATAGatggtgagcaagggcgagga and T7_citrine_R:

TAATACGACTCACTATAGGGcttgtacagctcgtccatgc; SP6_mcherry_ish_F:

GATTTAGGTGACACTATAGatggtgagcaagggcgag and T7_mcherry_ish_R:

TAATACGACTCACTATAGGGttacttgtacagctcgtcca) and purified. Anti-sense riboprobe was synthesized with T7 polymerase. NBT/BCIP was used as a chromogenic substrate for color *in situs.* For double fluorescent *in situ* hybridizations, probes were labeled with *digoxigenin* or *fluorescein*, and sequentially detected with anti-DIG or anti-Fluor POD-conjugated antibody for development with Tyramide Signal Amplification Plus Cyanine 3 or Fluorescein kits (Perkin-Elmer).

Immunohistochemistry was performed on whole mount embryos. Embryos were subsequently embedded in 17% gelatin in PBS and fixed in 4% paraformaldehyde in PBS for vibratome sectioning. We used rabbit anti-GFP antibody (Invitrogen) at 1:300, anti-rabbit Alexa488 (Invitrogen) at 1:1000, and rhodamine phalloidin (Molecular Probes) at 1:100. Sections were imaged on a Zeiss Pascal confocal microscope.

Confocal live imaging

Live embryos were mounted in 1% low-melting agarose with Tricaine in 30% Danieau solution (17 mM NaCl, 0.21 mM KCl, 0.12 mM $MgSO_4$, 0.18 mM $Ca(NO_3)_2$, 1.5 mM HEPES pH 7.6) for confocal imaging. For time-lapse imaging, embryos were injected at the single-cell stage with 40 pg of *h2b-cerulean* and 40 pg of membrane-tagged *mcherry* mRNA, synthesized with SP6 mMessage mMachine kit (Ambion) from pCS2+ expression vectors. Heterozygous *Gt(foxd3-citrine)*^{ct110a} embryos were sorted for expression of Citrine. Sequential Z-stack series were obtained with a Zeiss LSM510 laser-scanning confocal microscope, using objective Zeiss 20X 0.8mm. For the analysis of the *Gt(foxd3-mcherry)*^{ct110aR} phenotype, embryos were imaged using a Zeiss 25X 0.8mm and 40X 1.1mm objectives. Citrine signal was excited with a 514 nm laser, mCherry with 561 nm laser and Cerulean with a 458 nm laser.

Analysis of time-lapse

Datasets were analyzed with Imaris software. Co-localization of Citrine signal (FoxD3-Citrine) with H2B-Cerulean was used to define “spots” representing the position of neural crest cells as a function of time. Displacement length was calculated as the distance in micrometers between the initial and final position for each cell track. The net directional movement of NCCs was calculated for the cranial neural crest cells situated in the left side

of the embryo as the resultant vector of the individual trajectories and normalized for the number of cell tracks in each region analyzed.

RESULTS

We present a zebrafish line *ct110a*, with specific expression of Citrine in neural crest (NC) cells. The line was isolated from a FlipTrap Tol2-mediated gene trap and protein fusion screen (Trinh et al., 2011). The gene trap cassette includes the sequence of *citrine*, flanked by zebrafish *rassf8* splice acceptor (5′) and donor (3′) sites. When the cassette is integrated into an intronic region, *citrine* is transcribed as an artificial exon and spliced to generate a fusion protein (Fig. 1A).

Expression of Citrine fusion protein reflects neural crest cell distribution in ct110a embryos

In *ct110a* embryos, Citrine is first observed at the 1–2 somite stage (ss), as bilateral patches of expression at the neural plate border. At 6 ss, Citrine expression at the dorsolateral edges of the neural keel extends to the dorsal neural tube (Fig. 1B), but also can be detected at low levels in the ventral midline, particularly in the floor plate (Fig. 1B,F). At 14 ss, expression of Citrine corresponds to distribution of NC cells as they delaminate from the neural tube (Fig. 1C,G,K), and extensively migrate towards their final destination in the embryo (Fig. 1D). Figure 1E shows migration of cranial neural crest to the head and around the eyes. Citrine is expressed in both premigratory (Fig. 1F) and migrating forebrain, midbrain and rostral hindbrain neural crest (Fig. 1G,K), as well as in segregated populations of NC in the r2, r4 and r6 streams (Fig. 1H,L).

Citrine is expressed under the endogenous regulation of FoxD3

To determine the genomic insertion of the FlipTrap construct, we performed splinkerette-PCR. The results show that the FlipTrap vector had inserted into chromosome 6, within the coding region of *foxd3*, immediately upstream of the forkhead domain (position 300 of the coding region) (Fig. 2A). Moreover we found that, consistent with previous reports, Tol2-mediated integration resulted in duplication of a short region of 8 bp of the *foxd3* sequence flanking the site of integration (Kondrychyn et al., 2009).

To analyze the transcriptional outcome of *ct110a* integration, we performed 5′ and 3′ RACE PCR. 5′ RACE PCR reveals the presence of a fusion transcript consisting of the 5′ portion of *foxd3* and the *citrine* artificial exon. The gene trap cassette is integrated into the only exon of the *foxd3* gene. Presence of a cryptic splice donor site at position 276–290 (cagcctg***gt***aaagcc, score 0.88, http://www.fruitfly.org/seq_tools/splice.html) results in interaction with the splice acceptor site in the FlipTrap construct (Fig. 1A), fusing Citrine to the N-terminal portion of FoxD3. This splicing event disrupts the Forkhead domain of FoxD3 protein (Fig. 2A). We refer to this line as *Gt(foxd3-citrine)*^{ct110a}.

To form a stable functional fusion transcript, the splice donor site after the *citrine* sequence was designed to recognize splice acceptor sites located downstream of the insertion site (Trinh et al., 2011). 3′ RACE using a *citrine* gene-specific primer showed that the *citrine* artificial exon of the *ct110a* line alternatively splices into exons 2, 3 or 9 of *alg6*, the next downstream gene, which is separated from *foxd3* by a 5kb intergenic region (Fig. 2A). Figure 2B shows the identified splicing products for *Gt(foxd3-citrine)*^{ct110a}. Splicing into exons 2 and 3 results in a frame shift, generating a premature stop signal in the beginning of the sequence of *alg6*. The resulting fusion proteins contain a short Alg6 tail of 2 or 19 amino acids, respectively. Splicing into exon 9 produces an Alg6 tail of 236 amino acids.

This splicing event produces a chimeric Citrine-fusion protein, consisting of the N-terminal portion of FoxD3 and an Alg6 tail, lacking nuclear localization signal (Fig. 3B). Cytoplasmic expression of Citrine in *ct110a* embryos is regulated by endogenous *foxd3* regulatory machinery and corresponds to the endogenous distribution of *foxd3* in wild type embryos during the stages of gastrula and early somitogenesis, as determined by whole mount *in situ* hybridization (Fig. 2C–F). Expression of *citrine* and *foxd3* persists in the branchial arches and in migrating NC cells in the head as assessed by double fluorescent *in situ* hybridization for *foxd3* in wild type embryos as well as using a *citrine* probe in the *Gt(foxd3-citrine)*^{ct110a} line (Fig. 2G–I).

Dynamic analysis of neural crest migration

Despite splicing events that alter the coding region of *foxd3*, heterozygous *Gt(foxd3-citrine)*^{ct110a} embryos develop normally. Importantly, cytoplasmic distribution of FoxD3-Citrine fusion protein, due to the loss of nuclear localization signal, makes this line a particularly useful tool to visualize migratory behavior of neural crest cells. Moreover, reflecting the endogenous distribution of FoxD3 protein, Citrine expression initiates considerably earlier than other zebrafish neural crest transgenic lines generated to date, allowing access to early steps in neural crest formation.

In zebrafish, convergence and extension movements progressively transform the initially flat neural plate into a neural keel, and subsequently into a neural rod. Changes in cell adhesion result in cavitation, giving rise to the lumen of the neural tube. These changes are closely linked to progressive formation of neural crest. Employing time-lapse confocal microscopy using the *Gt(foxd3-citrine)*^{ct110a} line, it is possible to follow dynamic aspects of cell behavior by tracking individual cells and analyzing movements and intercellular interactions along neural crest migratory pathways. To follow NC cells from the earliest stages of FoxD3 expression, we took advantage of the low levels of Citrine expression in the floor plate to sort positive embryos at the end of gastrulation. This allowed us to capture Citrine expression in newly-induced crest cells from the earliest stages, and follow the expansion of Citrine expression along the neural plate border, as well as the dynamics of neural crest delamination and migration (Fig. 3, Movie 1).

Our results show that Citrine expression is first detected in a thickened area at the lateral borders of the anterior neural plate (Fig. 3A). Convergence and extension movements result in narrowing of the neural plate into a neural keel. Expression of FoxD3 initiates in the anterior-lateral borders of the neural plate, and progresses posteriorly with an increase in the number of Citrine-positive neural crest cells still localized in the neural plate border (Fig. 3B). Shortly thereafter, expression of FoxD3 is detected on the dorsal aspect of the neural keel, as a consequence of the dynamic movement of a subset of neural crest precursors first towards the midline, and then back to the sides of the neural tube. These opposing movements may correspond to neural tube closure and onset of migration, respectively, in amniotes (Colas and Schoenwolf, 2001), though in zebrafish neural tube formation depends upon convergent extension (Ciruna et al., 2006). Expression of Citrine strengthens with time, and segmentation of the NC field arises along the anterior-posterior axis (Fig. 3C). These furrows align with sites from which NC cells subsequently move and converge toward the midline (Fig. 3D). In Figure 3E, neural crest cells have migrated back to the sides of the neural tube. There is a clear segmental arrangement of mesenchymal cranial crest cells that migrate anteriorly, and those that migrate toward the branchial arches in pre- and post-otic regions (Fig. 3F).

High-resolution time-lapse imaging affords cellular resolution, allowing tracking of individual cell movement (Fig. 3G–J). To obtain 4-dimensional cellular resolution of neural crest behavior in the context of the whole embryo, we injected heterozygous *Gt(foxd3-*

citrine)^{ct110a} embryos with mRNA encoding membrane-tagged mCherry and nuclear localized H2B-Cerulean. Using the co-localization of Citrine and H2B-Cerulean as a dual-system for tracking of individual crest cells, we assessed the speed and displacement length of cranial neural crest cells. Moreover, we analyzed the net migratory movement of neural crest as a vector sum of individual migratory trajectories, normalized for the number of trajectories analyzed. Using these quantitative criteria to analyze the migratory movements of neural crest, we characterized four distinct phases of NC migratory behavior in zebrafish (Fig. 3K–P).

FoxD3-positive NC cells emerge at the neural plate border as two bilateral fields, initiating a first wave of migratory movement to the midline that is associated with convergent extension of the neural plate. Our analysis of the migratory trajectories indicates that the net movement of the posterior region of the crest field is aligned in the equatorial plane, while the cells in the rostral end migrate anteriorly (Fig. 3K). During this phase, neural crest cells migrated at an average speed of 19.2±0.4 nm/s (average±s.e.m.) (n=597 points) (Fig. 3K). This migratory movement persists during Phase II, as NC cells continue to migrate anteriorly and to the midline. During this phase, crest cells migrate faster with an average speed of 22.9±0.4 nm/s (n=2132 points) (Fig. 3O). In particular, our quantitative analyses of the migratory trajectories showed that the neural crest field encompasses three migratory patterns during Phase II: (1) posterior cells that migrate extensively to the midline with a net displacement of 34.4 μm, (2) anterior crest cells migrating anteriorly, and (3) a middle field of NC cells with a intermediate directional vector and the shortest net displacement of 23.5 μm (Fig. 3L). In Phase III, the posterior cells reverse their direction and move laterally away from the midline. Their trajectories increase in complexity and we can identify a retrograde anterior-lateral movement of cells toward the branchial arches (Fig. 3M). In the anterior crest field, cells migrate forward towards the head. During this third phase, displacement is significantly reduced: NC cells migrate an average distance of 18.0±0.6 μm (n=588 tracks), and their average speed is 18.2±0.2 nm/s (n=3424 points). Finally, NC cells condense into a characteristic segmental arrangement entering the branchial arches to undergo subsequent differentiation (Fig. 3N). During Phase IV, the average speed of NC cells is 10.2±0.1 nm/s (n=6522 points) and their average track length is 14.4±0.4 μm (n=644 tracks).

Cre recombination of the ct110a line produces a FoxD3-mCherry line

The FlipTrap construct contains, in an inverted direction, a *mcherry* sequence with a stop signal followed by zebrafish *alpha-tubulin polyA* (pA), flanked by *loxPV* sites (Trinh et al., 2011). An additional pair of *loxP* sites is arranged outside *citrine* and *mcherry*. In the presence of the Cre enzyme, these heterotypic loxP sites recombine, excising *citrine* and the splicing donor, such that *mcherry-pA* is flipped into a functional position, causing premature termination of the tagged protein (Fig. 4A).

Using Cre-loxP recombination, we generated a clean FoxD3 mutant line *Gt(foxd3-mcherry)*^{ct110aR}, in which the construct does not interfere with the downstream sequence of *alg6*. In the *Gt(foxd3-mcherry)*^{ct110aR} line, the FoxD3-mCherry fusion protein is terminated by the stop signal in the mCherry sequence and expressed under endogenous *foxd3* regulatory control (Fig. 4A).

Similarly to Citrine expression in *Gt(foxd3-citrine)*^{ct110a}, the *mcherry* fusion corresponds to the endogenous expression of *foxd3* in neural crest cells, as determined by fluorescent double *in situ* hybridization at 20 hpf (Fig. 4B–D). At higher magnification, confocal imaging of cells in the branchial arches shows that *mcherry* and *foxd3* are co-expressed in NC cells (Fig. 4E–G). Both Citrine and mCherry reflect the distribution of NC cells in the *ct110a* lines, from their early stages of induction in the neural plate border, through delamination and migration to their final destinations in the embryo. Importantly, we also

observed that expression of the FoxD3-fusion proteins is turned off in the NC-derived cartilage of the jaws and in the sensory neurons of the DRG, indicating that the endogenous repression of FoxD3 in subpopulations of NC cells is also recapitulated in these lines.

To demonstrate the exquisite sensitivity of *ct110a* labeling crest and compare it with an existing *foxd3* transgenic line, we crossed *Gt(foxd3-mcherry)*^{ct110aR} fish with the *Tg(foxd3:GFP)* line, which expresses GFP under control of a −14kb *foxd3* promoter (Gilmour et al., 2002). Expression of mCherry in *Gt(foxd3-mcherry)*^{ct110aR} initiates in pre-migratory cells, prior to expression of GFP (Fig. 4H). At the 18-ss, NC cells have migrated to the branchial arches, and can be consistently visualized by expression of mCherry (Fig. 4I). In contrast, expression of GFP is heterogeneously distributed in the *Tg(foxd3:GFP)* line (Fig. 4H,J), with only limited expression in branchial arches (Fig. 4J,K). Thus, the *ct110a* line offers an earlier and complete readout of FoxD3-expressing neural crest cells.

Homozygosis of Gt(foxd3-mcherry)^{ct110aR} produces FoxD3 mutants

Heterozygotes for *ct110a* lines expressing Citrine or mCherry undergo normal development and are viable. However, homozygosis of these lines produces FoxD3 mutants with similar defects in a variety of crest-derived tissues, including the craniofacial skeleton, dorsal root ganglia (DRG) and body pigmentation (Fig. 5) (Curran et al., 2009; Lister et al., 2006; Montero-Balaguer et al., 2006; Stewart et al., 2006). Here, we take advantage of the endogenously regulated expression of FoxD3-mCherry fusion protein to directly assess the cell autonomous effects of FoxD3 loss-of-function on the morphogenesis of the FoxD3-expressing tissues.

In zebrafish, three streams of cranial NC cells migrate ventrally and populate the pharyngeal arches. The first arch (mandibular) forms the jaw, the second (hyoid) forms jaw supporting structures, and the last five form the branchial gill structures. In *Gt(foxd3-mcherry)*^{ct110aR}, mCherry-positive cells constitute the pharyngeal arches at 32 hpf (Fig. 5A,B). In heterozygous *Gt(foxd3-mcherry)*^{ct110aR} embryos (*ct110R/+*), FoxD3-mCherry expression nicely delineates the morphology of the pharyngeal arches (Fig. 5A). Using confocal microscopy for higher resolution imaging of FoxD3-expressing cells, NC cells in heterozygotes appear tightly packed within the pharyngeal arches, with some cells sparsely distributed around the brain vesicles, and in concentric circles on and around the eyes (Fig. 5B). In contrast, in *Gt(foxd3-mcherry)*^{ct110aR} homozygotes (*ct110R/ct110aR*) morphogenesis of the pharyngeal arches is impaired (Fig. 5C). In particular, the mandibular prominence of the first arch is atrophic and the first and second arches appear to be fused. The most posterior arches are also smaller. Interestingly, we observe increased number of mCherry-positive cells migrating to the eye region. In a confocal projection, these cells appear to have increased protrusions, indicating a more mesenchymal identity (Fig. 5D). In addition to the cells distributed in the eye region, cells with mesenchymal appearance also are seen in the midbrain and hindbrain areas.

The defect in shape and size of the jaws is similar to one of the most apparent features of the *sym1* FoxD3 mutant (Stewart et al., 2006). In fact, *ct110R/ct110aR* embryos can be identified at 4 dpf based on characteristic changes in the facial profile. In all mutant embryos analyzed, Meckel's cartilage projects abnormally ventrally (Fig. 5G) and the ceratohyal and hyosymplectic cartilage elements are atrophic and malformed, failing to project anteriorly (n=11). Moreover, the most posterior pharyngeal elements (cb I–V) are absent (n=3) or very weakly stained (n=8) in Alcian Blue preparations (Fig. 5H).

The DRGs are segmentally arranged bilaterally alongside the neural tube and contain sensory neurons and associated glia, both of which arise from FoxD3-positive neural crest progenitors. Onset of *neurogenin* expression is associated with downregulation of FoxD3

and specification of sensory neurons, while FoxD3 maintenance favors glial cells (McGraw et al., 2008). Accordingly, in heterozygotes, FoxD3-mCherry is expressed in DRG-associated glial cells along the trunk, as well as in subsets of cells in the spinal cord (Fig. 5I). In the DRG of homozygous *Gt(foxd3-mcherry)*^{ct110aR} mutant embryos (n=14), the glial cells are largely missing, and the segmental distribution of DRGs is disrupted (Fig. 5J).

Previous studies on FoxD3 function have reported smaller jaws and lack of DRG neurons and glia (Lister et al., 2006; Montero-Balaguer et al., 2006; Stewart et al., 2006). The *mos* and *foxd3*^{zdf10} mutants and FoxD3 morphants had a reduction in iridophore number, but no other defects in pigment cell types other than a delay in melanophore migration (Lister et al., 2006; Montero-Balaguer et al., 2006; Stewart et al., 2006). Here we show that the delayed migration is followed by a significant increase in the number of melanophores after loss of FoxD3 in *Gt(foxd3-mcherry)*^{ct110R} zebrafish mutants.

We analyzed the distribution and numbers of melanophores of *ct110aR* embryos at 30 hpf and 56 hpf. At 30 hpf, melanophores accumulate in the head region behind the otic vesicle (Fig. 5K,K′), from where they migrate in a stream over the yolk (Fig. 5L). At this time, we observed consistent reduction in melanophores behind the ear (Fig. 5M,M′) or migrating over the yolk in homozygous ct110aR (n=10) (Fig. 5N) when compared to heterozygotes, in line with a previously reported delay in early melanophore migration (Stewart et al., 2006). Interestingly, at 56 hpf we observed an apparent increase in melanophore number in homozygous *Gt(foxd3-mcherry)*^{ct110aR} embryos, distributed in the dorsal and lateral sides of the body (Fig. 5O–R,S). At dorsal trunk levels, melanophores can be individually identified as bilateral groups of cells along the midline (Fig. 5O). In *ct110aR/ct110aR* mutants, however, these cells cover a large area of the dorsal midline and their edges cannot be distinguished (Fig. 5Q). Melanophores are also distributed along the lateral line. In *ct110R/+* embryos (n=20), these cells are more prevalent in the trunk (n=8.2±0.7) than in the tail (n=1.6±0.3) ($P<0.0001$) (Fig. 5P), and assume a flattened morphology (Fig. 5P′). In *c110aR* homozygotes, the number of melanophores is increased (18.3±0.9; n=14) compared with heterozygotes (n=9.85±0.6; n=20) (P=0.001), particularly in the tail at 56 hpf (Fig. 5R), and at 3 dpf, with 21.8±1.9 cells in *ct110R/ct110aR* embryos (n=10), compared to wild type (7.3±1.1, n=7) or heterozygotes (10.1±0.9, n=16). Moreover, melanophores in homozygotes show extensive cytoplasmic projections and are displaced from the midline (Fig. 5R′). As reported previously, the number of iridophores was significantly reduced in *ct110R/ct110aR* embryos, with 1.8±0.6 cells (mean±s.e.m.) per embryo ($P<0.0001$) compared with wild type (12.9±1.0; n=6) and heterozygotes (12.1±0.8; n=17), respectively, in the dorsal trunk at 52 hpf (Fig. 5T).

DISCUSSION

In this study, we present a novel zebrafish gene trap line *Gt(foxd3-citrine)*^{ct110a} that expresses Citrine as a fusion protein with FoxD3. Our results show that expression of Citrine fully recapitulates endogenous cellular distribution of FoxD3, making this line well-suited for assessing the dynamic behavior of neural crest cells in living embryos. By performing Cre-recombination, we obtained a variant of this line, *Gt(foxd3-mcherry)*^{ct110aR} which encodes a truncated FoxD3 protein fused to mCherry. Analysis of mCherry-positive cells in FoxD3 mutants, obtained by homozygosis of ct110aR, provides a novel approach to visualize the effects of *foxd3* knockdown at the cellular level.

Ct110a line as a resource for dynamic analysis of neural crest cell movement

Formation of the neural plate border and the subsequent transition from premigratory to migrating neural crest is thought to involve a stepwise and intricate gene regulatory network of induction and specification signals, including neural plate border and neural crest

specifier genes. Together, these factors instruct precursor cells of initially multipotent cells to undergo an epithelial-to-mesenchymal transition and leave the neural primordium. Neural crest cells acquire motility, migrate extensively throughout the embryo and adopt very distinct cell fates.

A particular advantage of using zebrafish for studies of dynamic cell movements is the ability to perform high-resolution live imaging. In the *Gt(foxd3-citrine)*^{ct110a} line, endogenously regulated expression of the fluorescent fusion protein exquisitely labels the nascent neural crest population. Using this line, we can visualize behavior of neural crest precursors expressing FoxD3 from times of early induction at the neural plate border, thus filling a gap in the current set of tools available for studying the neural crest. While transgenic neural crest lines, such as *Tg(-4.9sox10:EGFP)* (Carney et al., 2006) and *Tg(foxd3:GFP)* (Gilmour et al., 2002) have been remarkably useful, they do not recapitulate early steps in neural crest development (Carney et al., 2006; Gilmour et al., 2002; Wada et al., 2005). In these cases, the missing regulatory elements in the exogenous promoters or the genomic integration site may yield biased or incomplete expression patterns, such as delayed onset of reporter expression or restriction to a subpopulation of neural crest cells. Moreover, because Citrine and mCherry are expressed as a fusion to endogenous FoxD3, these lines also recapitulate the complex regulation of FoxD3, and are repressed in some subpopulations of crest derivatives.

In addition to neural crest cells, expression of *foxd3* has been previously described in the embryonic shield, floor plate, tailbud, somites, and at later stages, in a subset of cells in the hindbrain and spinal cord, lateral line, cranial ganglia and pineal gland (Kelsh et al., 2000; Lister et al., 2006; Odenthal and Nusslein-Volhard, 1998). In *ct110a* lines, expression of *citrine* and *mcherry* fully recapitulates the endogenous expression of *foxd3*. The splicing events, however, result in loss of the C-terminal part of the FoxD3 protein that includes the forkhead domain and nuclear localization signal, which target FoxD3 transcription factor to the nucleus. Hence, we take advantage of the cytoplasmic distribution of the fluorescent fusion protein to visualize the whole neural crest cells and analyze their dynamic migratory behavior from neural keel stage to active phases of cell migration.

Contextualizing neural crest development in zebrafish

In mouse and chick embryos, apical constriction of the lateral neural plate results in two hinge points that form the neural folds (Colas and Schoenwolf, 2001). During neurulation, morphogenetic forces from the non-neural ectoderm drive rotation of the neuroepithelium around the lateral hinge points, elevating the neural folds and bringing neural crest precursors to the dorsal aspect of the neural tube. In zebrafish, neurulation also involves folding of the neural plate towards the midline (Ciruna et al., 2006; Hong and Brewster, 2006). However, this morphogenetic movement results in apposition of apical surfaces from the contralateral neural plate; an active protrusive movement of radial convergence of the neuroepithelium results in formation of a neural keel. Organization of the midline takes place as cells intercalate into a neural rod (Hong and Brewster, 2006).

The novel FoxD3 line presented here provides a valuable tool to assess *in vivo* the role of different signaling pathways in the migratory behavior of neural crest cells. We observe that FoxD3-expressing neural crest precursors are initially present in the neural plate border; a subset of these cells moves toward the midline, during the neural keel stage, in a collective cell movement of convergent extension. In contrast to avian embryos, whose dorsal neural folds fuse bringing all neural crest to the dorsal midline, only a subset of zebrafish cells reach the midline before the emigration onset.

The *ct110* line enables direct analysis of FoxD3 loss-of-function

Using Cre-mediated recombination enabled by the FlipTrap approach, we obtained a mutant line that offers the advantage of allowing observation and direct analysis of the effects of FoxD3 loss in the same cells that would normally express it, via visualization of FoxD3-mCherry expression. Our results confirm previous findings showing that FoxD3 is essential for formation of crest-derived cartilage, glial cells associated with DRG and pigment cells, while simultaneously revealing new features of the phenotype. The defects caused by FoxD3 loss-of-function are consistent with those previously described in *foxd3* mutants or morphants: (1) $sym1^{zdf10}$ caused by a frame shift and premature truncation of the protein at the end of the forkhead DNA-binding domains (Stewart et al., 2006), (2) *mother superior* (mos^{m188}) (Montero-Balaguer et al., 2006) and (3) morpholino-mediated knockdown of FoxD3 protein (Lister et al., 2006).

In our line, FoxD3 loss results in severe reductions of the pharyngeal skeleton accompanied by a ventral displacement of Meckel's cartilage, and reduced or absent hyosymplectic and ceratohyal in the majority of embryos (Lister et al., 2006; Montero-Balaguer et al., 2006; Neuhauss et al., 1996; Stewart et al., 2006). These later effects are intriguing given that expression of *foxd3* is downregulated in neural crest cells that will form the craniofacial skeleton. The reduction in cell number in pharyngeal arches was previously analyzed using markers such as dlx2 and dlx8. Using the *ct110R* line to visualize cranial neural crest cells migrating to the pharyngeal arches, we can directly observe that the craniofacial defect is secondary to early impaired cranial crest specification and migration events caused by loss of FoxD3, with FoxD3 mutant cells appearing more mesenchymal and ectopically distributed in the head at 32hpf.

Although the most severe effects of FoxD3 loss involve later differentiating derivatives, our analysis provides the resolution to assess early effects of FoxD3 loss-of-function on cell behavior. The results provide a new approach to analyze an essential role for FoxD3 in early neural crest development and show that FoxD3 is important for acquisition of neural crest identity.

Role of FoxD3 in melanocyte development

FoxD3 has been shown to repress melanogenesis in chick embryos (Kos et al., 2001). However, regulation of melanogenesis by FoxD3 in zebrafish has been a matter of controversy (Lister et al., 2006; Montero-Balaguer et al., 2006; Stewart et al., 2006).

Consistent with previous studies, our analysis of melanocyte distribution in zebrafish indicates that lack of FoxD3 results in an initial reduction of melanoblasts at 30 hpf. We hypothesize that this reflects the early role of FoxD3 in specification of neural crest precursors. Subsequently, however, there is a significant increase in the number of melanophores in ct110aR mutant embryos. One possibility is that this could result from a delay in migration of melanophores. Alternatively, it may suggest that FoxD3 loss-of-function results in increased melanophores, thus reconciling the zebrafish data with that described in chick.

Consistent with the possibility that lack of FoxD3 results in increase in pigmentation, FoxD3 has been shown to repress Mitfa in zebrafish (Curran et al., 2009). MITF (microphthalmia-associated transcription factor) is essential for melanogenesis, transactivating expression of many of the genes required for melanin production and melanocyte differentiation and survival (Levy et al., 2006). FoxD3 is a transcriptional repressor proposed to act as a switch between glial precursors and pigment cell fates, by preventing Mitf from being expressed in the neural tube and in migrating neural and glial precursors (Curran et al., 2009; Ignatius et al., 2008; Thomas and Erickson, 2009). Moreover, interaction between *foxd3* and *mitfa* also

is required for the fate decision between melanophore and iridophore identities in zebrafish (Curran et al., 2010). These pigment cells descend from a common precursor and a reactivation of FoxD3 expression in these cells directs a subpopulation into an iridophore fate. In the absence of inhibition by FoxD3, however, Mitfa expression induces melanogenesis. A possible explanation for our observed phenotype is that, in the absence of FoxD3, there may be a lineage switch such that an increase in the number of melanophores occurs at the expense of both sensory glia and iridophores.

Our findings are consistent with previous studies in *foxd3* zebrafish mutants *mos* and *foxd3*^{zdf10} reporting an initial delay in melanoblast migration; however, the number of melanophores was not significantly affected (Montero-Balaguer et al., 2006; Stewart et al., 2006). Moreover, morpholino knockdown of *foxd3* resulted in even more subtle melanophore phenotypes (Ignatius et al., 2008; Lister et al., 2006). The contrasting observations in zebrafish could be associated with partial *foxd3* knockdown in previous studies. Consistent with this, Chang and Kessler have recently identified a residual Foxd3 activity in the *sym1* mutant, suggesting this is a hypomorphic allele of *foxd3* (Chang and Kessler, 2010). Alternatively, additional repressors for *mitfa* could be modulating the effect of FoxD3 loss-of-function (Curran et al., 2009).

Conclusions

Here, we describe a gene/protein trap line *gt(foxd3)*^{ct110a} in zebrafish that expresses a Citrine fusion protein with FoxD3, a transcription factor expressed in premigratory and migrating neural crest cells. Taking advantage of the endogenous FoxD3 regulatory machinery, combined with the versatility of the gene trap construct (Trinh et al., 2011), we present this line as a very robust resource for the study of neural crest specification and migration. By performing Cre-loxP recombination, we generated a zebrafish FoxD3 mutant line, in which endogenously regulated expression of a truncated FoxD3 is fused with mCherry, and allows *in vivo* analysis of the mutant phenotype, thus providing a novel approach to visualize the effects of *foxd3* knockdown at cellular resolution. Taken together, our results reveal new insights and advance the set of available tools to study the cellular mechanisms involved in specification and migration of neural crest cells.

Supplementary Material

Refer to Web version on PubMed Central for supplementary material.

Acknowledgments

We thank L. Trinh, T. Sauka-Spengler and M. Simões-Costa for comments on the manuscript and helpful discussions, Tom Schilling for sharing *foxd3* probe and *Tg(FoxD3:EGFP)* line, Leigh Ann Fletcher for fish care, Ilana Solomon, Neha Das and Joanne Tan for technical support and Daniel Koo for help with vector analysis. T.H. was supported by a Pew Latin American Fellowship in Biomedical Sciences and by California Institute for Regenerative Medicine Training Grant (T2-00006). This work was supported by NIH grants HG004071 and HD037105 (M.E.B).

References

Bang AG, Papalopulu N, Goulding MD, Kintner C. Expression of Pax-3 in the lateral neural plate is dependent on a Wnt-mediated signal from posterior nonaxial mesoderm. Developmental biology. 1999; 212:366–380. [PubMed: 10433827]

Basch ML, Bronner-Fraser M, Garcia-Castro MI. Specification of the neural crest occurs during gastrulation and requires Pax7. Nature. 2006; 441:218–222. [PubMed: 16688176]

Carney TJ, Dutton KA, Greenhill E, Delfino-Machin M, Dufourcq P, Blader P, Kelsh RN. A direct role for Sox10 in specification of neural crest-derived sensory neurons. Development. 2006; 133:4619–4630. [PubMed: 17065232]

Chang LL, Kessler DS. Foxd3 is an essential Nodal-dependent regulator of zebrafish dorsal mesoderm development. Developmental biology. 2010; 342:39–50. [PubMed: 20346935]

Ciruna B, Jenny A, Lee D, Mlodzik M, Schier AF. Planar cell polarity signalling couples cell division and morphogenesis during neurulation. Nature. 2006; 439:220–224. [PubMed: 16407953]

Clevidence DE, Overdier DG, Tao W, Qian X, Pani L, Lai E, Costa RH. Identification of nine tissue-specific transcription factors of the hepatocyte nuclear factor 3/forkhead DNA-binding-domain family. Proceedings of the National Academy of Sciences of the United States of America. 1993; 90:3948–3952. [PubMed: 7683413]

Colas JF, Schoenwolf GC. Towards a cellular and molecular understanding of neurulation. Developmental dynamics: an official publication of the American Association of Anatomists. 2001; 221:117–145. [PubMed: 11376482]

Curran K, Lister JA, Kunkel GR, Prendergast A, Parichy DM, Raible DW. Interplay between Foxd3 and Mitf regulates cell fate plasticity in the zebrafish neural crest. Developmental biology. 2010; 344:107–118. [PubMed: 20460180]

Curran K, Raible DW, Lister JA. Foxd3 controls melanophore specification in the zebrafish neural crest by regulation of Mitf. Dev Biol. 2009; 332:408–417. [PubMed: 19527705]

Gilmour DT, Maischein HM, Nusslein-Volhard C. Migration and function of a glial subtype in the vertebrate peripheral nervous system. Neuron. 2002; 34:577–588. [PubMed: 12062041]

Hong E, Brewster R. N-cadherin is required for the polarized cell behaviors that drive neurulation in the zebrafish. Development. 2006; 133:3895–3905. [PubMed: 16943271]

Ignatius MS, Moose HE, El-Hodiri HM, Henion PD. colgate/hdac1 Repression of foxd3 expression is required to permit mitfa-dependent melanogenesis. Developmental biology. 2008; 313:568–583. [PubMed: 18068699]

Kelsh RN, Dutton K, Medlin J, Eisen JS. Expression of zebrafish fkd6 in neural crest-derived glia. Mech Dev. 2000; 93:161–164. [PubMed: 10781949]

Knecht AK, Bronner-Fraser M. Induction of the neural crest: a multigene process. Nat Rev Genet. 2002; 3:453–461. [PubMed: 12042772]

Kondrychyn I, Garcia-Lecea M, Emelyanov A, Parinov S, Korzh V. Genome-wide analysis of Tol2 transposon reintegration in zebrafish. BMC Genomics. 2009; 10:418. [PubMed: 19737393]

Kos R, Reedy MV, Johnson RL, Erickson CA. The winged-helix transcription factor FoxD3 is important for establishing the neural crest lineage and repressing melanogenesis in avian embryos. Development. 2001; 128:1467–1479. [PubMed: 11262245]

Labosky PA, Kaestner KH. The winged helix transcription factor Hfh2 is expressed in neural crest and spinal cord during mouse development. Mechanisms of development. 1998; 76:185–190. [PubMed: 9767163]

Le Douarin, N.; Kalcheim, C. The neural crest. 2. Cambridge University Press; New York: 1999.

Levy C, Khaled M, Fisher DE. MITF: master regulator of melanocyte development and melanoma oncogene. Trends Mol Med. 2006; 12:406–414. [PubMed: 16899407]

Lister JA, Cooper C, Nguyen K, Modrell M, Grant K, Raible DW. Zebrafish Foxd3 is required for development of a subset of neural crest derivatives. Dev Biol. 2006; 290:92–104. [PubMed: 16364284]

McGraw HF, Nechiporuk A, Raible DW. Zebrafish dorsal root ganglia neural precursor cells adopt a glial fate in the absence of neurogenin1. J Neurosci. 2008; 28:12558–12569. [PubMed: 19020048]

Monsoro-Burq AH, Wang E, Harland R. Msx1 and Pax3 cooperate to mediate FGF8 and WNT signals during Xenopus neural crest induction. Developmental cell. 2005; 8:167–178. [PubMed: 15691759]

Montero-Balaguer M, Lang MR, Sachdev SW, Knappmeyer C, Stewart RA, De La Guardia A, Hatzopoulos AK, Knapik EW. The mother superior mutation ablates foxd3 activity in neural crest progenitor cells and depletes neural crest derivatives in zebrafish. Dev Dyn. 2006; 235:3199–3212. [PubMed: 17013879]

Neuhauss SC, Solnica-Krezel L, Schier AF, Zwartkruis F, Stemple DL, Malicki J, Abdelilah S, Stainier DY, Driever W. Mutations affecting craniofacial development in zebrafish. Development. 1996; 123:357–367. [PubMed: 9007255]

Odenthal J, Nusslein-Volhard C. fork head domain genes in zebrafish. Dev Genes Evol. 1998; 208:245–258. [PubMed: 9683740]

Phillips BT, Kwon HJ, Melton C, Houghtaling P, Fritz A, Riley BB. Zebrafish msxB, msxC and msxE function together to refine the neural-nonneural border and regulate cranial placodes and neural crest development. Developmental biology. 2006; 294:376–390. [PubMed: 16631154]

Sato T, Sasai N, Sasai Y. Neural crest determination by co-activation of Pax3 and Zic1 genes in Xenopus ectoderm. Development. 2005; 132:2355–2363. [PubMed: 15843410]

Sauka-Spengler T, Bronner-Fraser M. A gene regulatory network orchestrates neural crest formation. Nat Rev Mol Cell Biol. 2008; 9:557–568. [PubMed: 18523435]

Stewart RA, Arduini BL, Berghmans S, George RE, Kanki JP, Henion PD, Look AT. Zebrafish foxd3 is selectively required for neural crest specification, migration and survival. Dev Biol. 2006; 292:174–188. [PubMed: 16499899]

Sutton J, Costa R, Klug M, Field L, Xu D, Largaespada DA, Fletcher CF, Jenkins NA, Copeland NG, Klemsz M, Hromas R. Genesis, a winged helix transcriptional repressor with expression restricted to embryonic stem cells. The Journal of biological chemistry. 1996; 271:23126–23133. [PubMed: 8798505]

Teng L, Mundell NA, Frist AY, Wang Q, Labosky PA. Requirement for Foxd3 in the maintenance of neural crest progenitors. Development. 2008; 135:1615–1624. [PubMed: 18367558]

Thisse C, Thisse B, Schilling TF, Postlethwait JH. Structure of the zebrafish snail1 gene and its expression in wild-type, spadetail and no tail mutant embryos. Development. 1993; 119:1203–1215. [PubMed: 8306883]

Thomas AJ, Erickson CA. FOXD3 regulates the lineage switch between neural crest-derived glial cells and pigment cells by repressing MITF through a non-canonical mechanism. Development. 2009; 136:1849–1858. [PubMed: 19403660]

Trinh LA, Hochgreb T, Graham M, Wu D, Ruf-Zamojski F, Jayasena CS, Saxena A, Hawk R, Gonzalez-Serricchio A, Dixson A, Chow E, Gonzales C, Leung HY, Solomon I, Bronner-Fraser M, Megason SG, Fraser SE. A versatile gene trap to visualize and interrogate the function of the vertebrate proteome. Genes & development. 2011; 25:2306–2320. [PubMed: 22056673]

Uren AG, Mikkers H, Kool J, van der Weyden L, Lund AH, Wilson CH, Rance R, Jonkers J, van Lohuizen M, Berns A, Adams DJ. A high-throughput splinkerette-PCR method for the isolation and sequencing of retroviral insertion sites. Nat Protoc. 2009; 4:789–798. [PubMed: 19528954]

Wada N, Javidan Y, Nelson S, Carney TJ, Kelsh RN, Schilling TF. Hedgehog signaling is required for cranial neural crest morphogenesis and chondrogenesis at the midline in the zebrafish skull. Development. 2005; 132:3977–3988. [PubMed: 16049113]

Westerfield, M. The Zebrafish Book: A Guide for the Laboratory Use of Zebrafish (Brachydanio rerio). University of Oregon Press; Eugene, OR: 1995.

Highlights

- A novel zebrafish gene trap line expressing Citrine-tagged endogenous FoxD3.
- Citrine expression recapitulates endogenous FoxD3 expression.
- Cre-recombination produces a FoxD3 mutant.
- Mutant expresses FoxD3-Cherry fusion protein.
- Cherry expression allows analysis of FoxD3 loss-of-function at cellular resolution.

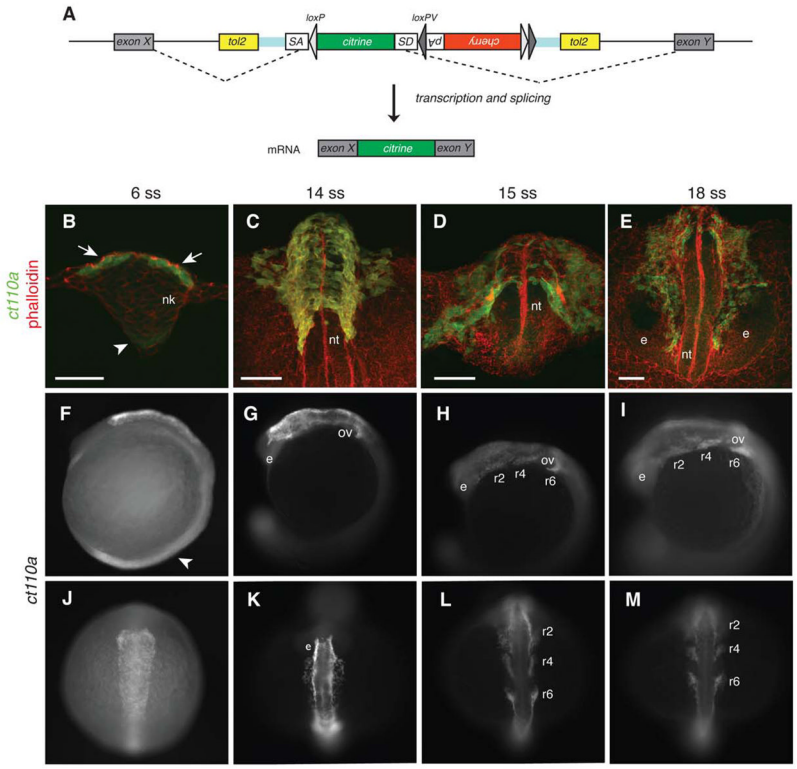

Figure 1. A novel protein trap line allows visualization of neural crest cells from early stages in zebrafish

(A) Schematic diagram of the FlipTrap strategy. The FlipTrap construct contains an internal exon, consisting of *citrine* sequence lacking start and stop codons (green), flanked by splice acceptor (*SA*) and donor (*SD*) sites. Genomic integration of the construct is mediated by Tol2 transposase. When the FlipTrap construct inserts within an intronic region, the endogenous splicing machinery recognizes SA and SD sites, and the *citrine* sequence is integrated into the mRNA (dashed lines), resulting in an endogenously expressed Citrine-fusion protein.

(B–D) Confocal images of *ct110a* embryos. Transverse sections. C–D are 3D-projections of z-stacks. Embryos counterstained with phalloidin-rhodamine (red) and Citrine signal amplified by immunohistochemistry against GFP after fixation (green). (B) Expression of Citrine is detected in the dorso-lateral cells (white arrow) of the neural keel (nk) at 6-somite stage (ss). Low-level expression can be detected in the floor plate (white arrowhead). (C) Delamination of neural crest cells (NCCs) from the neural tube (nt). Citrine-positive cells distributed on the dorsal aspect of the neural tube at 14ss. (D) Migration of NCCs from the neural tube along stereotyped routes throughout the embryo. (E) At 18ss, cranial NCCs migrate anteriorly to the head, circumventing the eyes (e). Scale bars: 50 μm.

(F–M) Expression of Citrine in *ct110a* embryos. (F–I) Left side view. (J–M) Dorsal view. Citrine signal amplified by GFP immunostaining in fixed embryos. (F,J) Expression of Citrine in NCCs on the dorsal aspect of the anterior neural tube, at the level of the hindbrain. Low expression in the floor plate region (white arrowhead). (G,K) NCCs delaminate and migrate from the neural tube to the head, around the otic vesicles (ov) and eyes (e). (H,I,L,M) NCCs migrate ventrally into the pharyngeal arches in three separate streams along stereotyped routes (r2, r4 and r6).

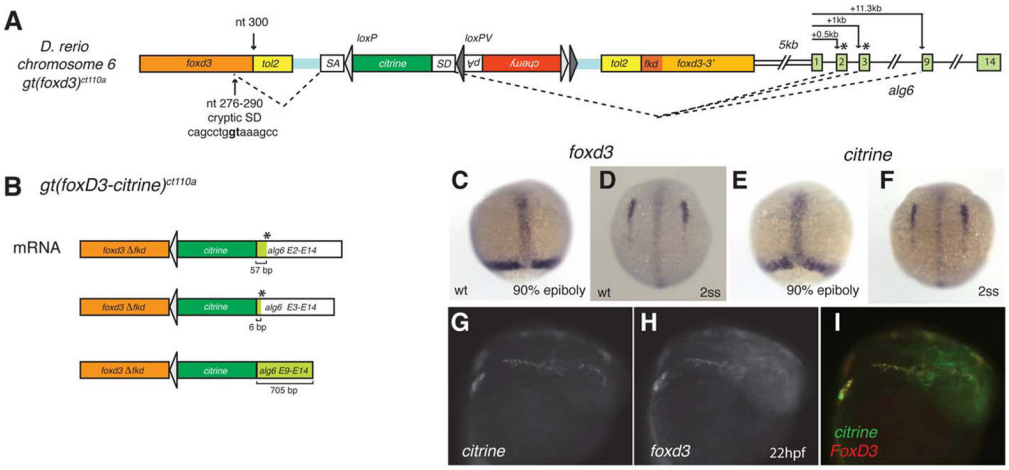

Figure 2. Expression of *citrine* in ct110a reflects endogenous expression of *foxd3*

(A) Schematic diagram of genomic FlipTrap integration in the *ct110a* line. Integration of the FlipTrap construct occurred within the coding region of *foxd3*, in chromosome 6. Splice acceptor site (*SA*) of the *citrine* internal exon recognizes a cryptic splice donor site within *foxd3* sequence (nucleotides 276–290 of *foxd3* coding sequence). The splice donor site (SD) of *citrine* reacts with acceptor sites of *alg6.* The *citrine* exon splices with exons 3 or 9 of *alg6*, respectively situated at +1kb or +11.3kb downstream from the *alg6* start site in the genomic sequence. (B) Splicing events produce a chimeric Citrine-fusion protein, which encodes the N-terminal portion of FoxD3 (FoxD3-ΔFkd) and an Alg6 tail. Splicing of *citrine* with exon 2 or 3 of *alg6* results in a short Alg6 tail (19 or 2 aminoacids, respectively), caused by a premature stop signal (*) generated by a frame shift. Alternative splicing with exon 9 does not affect the coding frame.

(C–I) Expression of *citrine* recapitulates *foxd3* expression in the *Gt(foxd3-citrine)*^{ct110a} line. Whole mount *in situ* hybridization to *foxd3* (C,D) and *citrine* (E,F). (C) Early expression of *foxd3* in the prechordal plate and blastoderm margin of zebrafish embryos in late gastrula. (D) *foxd3* expression by neural crest cells initiates during early somitogenesis, as bilateral fields in the anterior neural plate border.

(E,F) Distribution of *citrine* transcripts in *Gt(foxd3-citrine)*^{ct110a} embryos corresponds to endogenous expression of *foxd3*. (G–I) *citrine* mRNA co-localizes with *foxd3* endogenous expression in neural crest cells. Double fluorescent whole mount *in situ* hybridization to *citrine* and *foxd3* in *Gt(foxd3-citrine)*^{ct110a} embryos at 22 hpf.

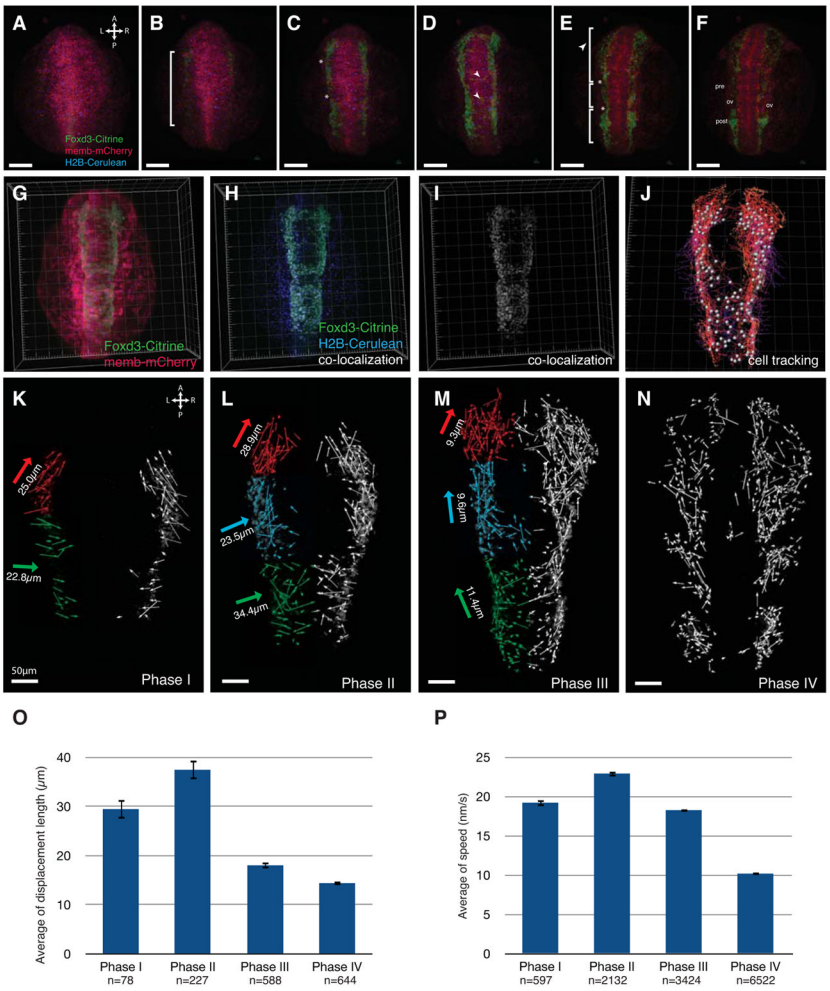

Figure 3. Analysis of the dynamics of neural crest migration in *ct110a* embryos

(A–F) Confocal projections of time-lapse imaging of live *Gt(foxd3-citrine)*^{ct110a} embryos. Dorsal views. Panels represent 1-hour intervals. FoxD3-Citrine signal is depicted in green; membrane-tagged mCherry, red; H2B-Cerulean, blue. (A) Onset of FoxD3-Citrine expression at the 1–2 somite stage as NCCs are induced in the anterior neural plate border. (B) Expansion of FoxD3-Citrine expression along the neural plate border. (C) Segmentation of the neural crest field is first delineated by the appearance of furrows (asterisks) along its rostral-caudal extent. (D) A subset of NC cells moves towards the midline (arrowheads) at specific anterior-posterior levels. (E) Citrine-positive cells return from the midline to the lateral aspect of the neural tube, migrate towards the head and branchial arches, where they will condense. (F) Consolidation of the rostral-caudal segmentation of cranial neural crest as they migrate anteriorly to the head region, or condense in pre- and post-otic ganglia. Scale bars, 100 μm.

(G–J) Cell tracking analysis of time-lapse dataset. Dorsal views. (G) Panel represents projection of a single time-point. (H,I) Co-localization of Citrine signal with H2B-Cerulean is depicted in white. (J) Tracing of NC migration obtained by tracking co-localization signal in a representative time-lapse dataset of *Gt(foxd3-citrine)*^{ct110a} embryos.

(K–P) Phases of the morphogenetic movements of cranial NCCs in zebrafish. (K–N) Projection of NC displacement trajectories analyzed for each phase. Dorsal views. Thin arrows represent the displacement vectors of NC cells. Thick arrows are the projection of the

resultant displacement unit vector, color-coded for each corresponding region. Resultant magnitude values are normalized for the number of trajectories and indicated in micrometers. Scale bars 50 μm. (K) Induction of NCCs in the neural plate border and initial migration to the midline. (L) Migration of NC to the midline and anteriorly. (M) NCCs migrate laterally and anteriorly towards the branchial arches and head. (N) Consolidation of NCCs position in branchial arches and head region for subsequent differentiation. (O) Quantitative analysis (mean±s.e.m.) showed that on average, displacement of cranial NC cells is significantly distinct during Phases I, II and III/IV. Displacement length between phases III and IV is not significant. ANOVA statistical test $P<0.0001$. (P) Quantitative analysis showed that NC migrate faster during Phase II, and slow down as cells migrate to their final destination for subsequent differentiation. Speed is significantly different among Phases I through IV. ANOVA test $p<0.0001$.

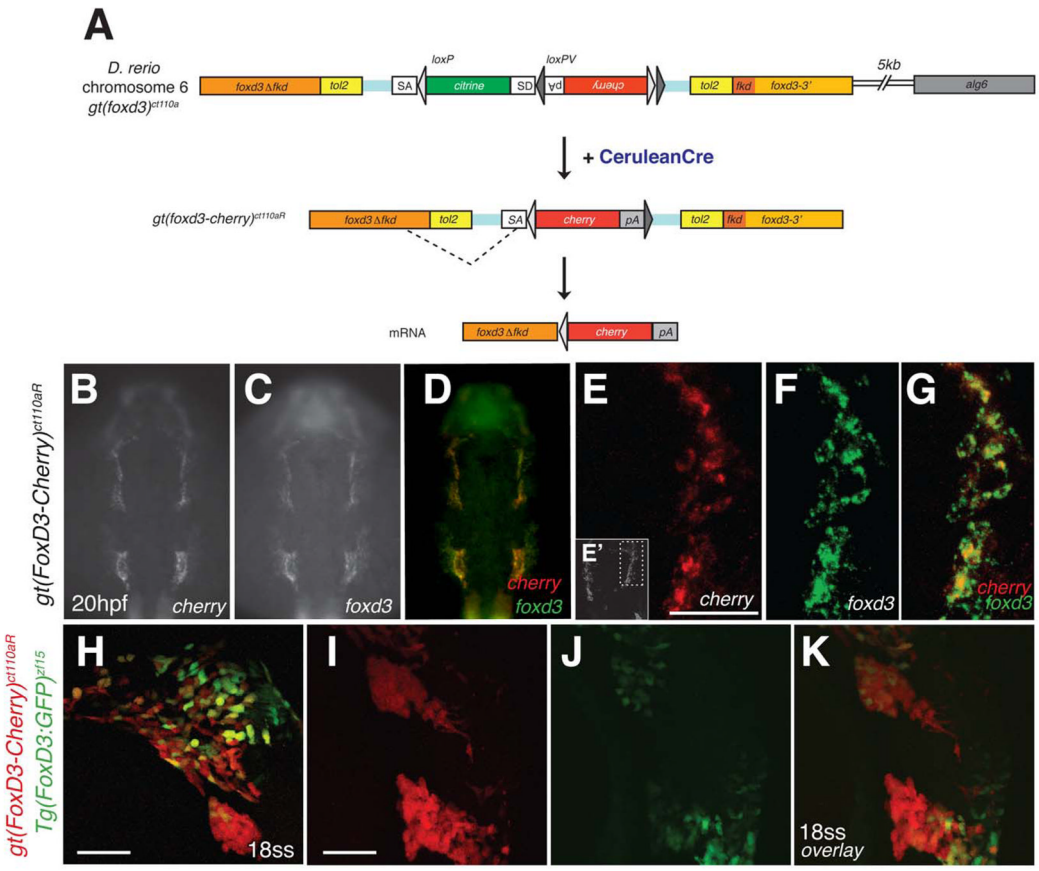

Figure 4. Cre-mediated recombination of *Gt(foxd3-citrine)*^{ct110a} results in expression of a mutant FoxD3-mCherry fusion protein

(A) Schematic diagram of Cre-loxP recombination in *Gt(foxd3-citrine)*^{ct110a} zebrafish line. The FlipTrap construct contains inverted mCherry (red box) and polyA (pA) sequences, flanked by heterotypic loxP (light gray) and loxPV (dark gray) sites. In embryos injected with *cerulean-cre* mRNA, recombination of the loxP sites results in deletion of *citrine* and correct orientation of *mcherry-pA*. Splicing of *foxd3* cryptic splice donor site with *mcherry* splice acceptor site (*SA*) produces a mutant FoxD3ΔFkd-mCherry fusion protein, expressed under *foxd3* endogenous regulation.

(B–K) Expression of *mcherry* co-localizes with endogenous *foxd3* in *Gt(foxd3-mcherry)*^{ct110R} embryos, whereas *Tg(foxd3:GFP)* line recognizes a subpopulation of NCCs. (B–G) Fluorescent whole mount *in situ* hybridization in *Gt(foxd3-mcherry)*^{ct110aR} embryos at 22 hpf. Expression of *mcherry* (B) is detected in the branchial arches, in the same distribution as endogenous *foxd3* (C,D). High-resolution confocal imaging of *mcherry* (red; E,G) and *foxd3* (green; F,G) shows co-expression in the branchial arches, as shown in the inset (E′, dashed line).

(H–K) Confocal imaging of double transgenic *Gt(foxd3-mcherry)*^{ct110aR}*; Tg(foxd3:GFP)* embryo at 18-somite stage. Expression of ct110aR (red) allows visualization of early NCCs associated with the neural tube (K) and NC in the branchial arches (H). In contrast to expression of FoxD3-mCherry, which comprehensively labels neural crest cells, expression of GFP (green) driven by a −14kb promoter is heterogeneously distributed (H,J) and shows restricted expression in the branchial arches at 18ss (J,K). Scale bars: 50 μm.

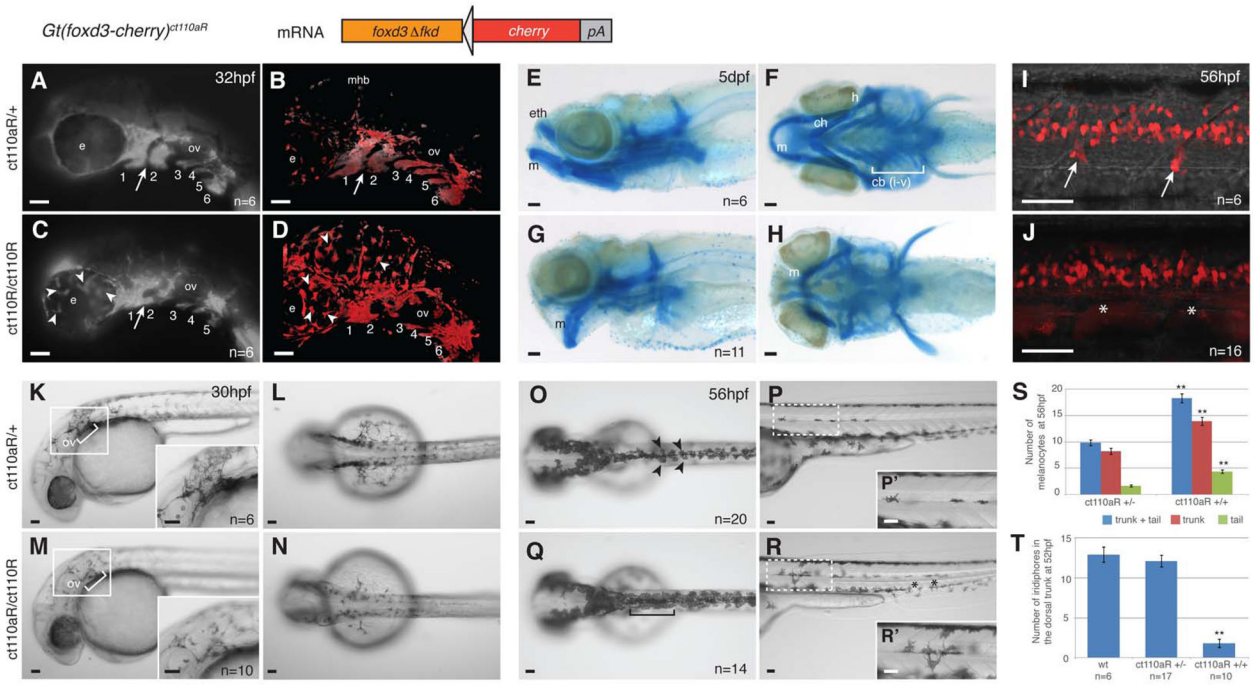

Figure 5. FoxD3 loss-of-function in *Gt(foxd3-mcherry)*^{ct110aR} homozygotes reveals multiple aspects of FoxD3 mutant phenotype

Development of *Gt(foxd3-mcherry)*^{ct110aR} heterozygotes (ct110aR/+) is normal. Homozygosis (ct110aR/ct110aR) results in a FoxD3 mutant phenotype.

(A–D) Loss of FoxD3 affects migration of NCCs to the pharyngeal arches. 6 embryos with each genotype were live imaged and analyzed, showing similar phenotypes. Lateral views, anterior to the left. (A,C) Images of mCherry fluorescence in the head of *Gt(foxd3-mcherry)*^{ct110aR} embryo. (B,D) Confocal projections of *Gt(foxd3m-mcherry)*^{ct110aR} embryos head region. Expression of FoxD3-mCherry allows visualization of NCCs in the branchial arches of *Gt(foxd3-mcherry)*^{ct110aR} embryos. (A) Normal development and segmentation of pharyngeal arches (1–6) in *Gt(foxd3-mcherry)*^{ct110aR} heterozygotes. (B) Confocal imaging of *Gt(foxd3-mcherry)*^{ct110aR} heterozygous embryo shows FoxD3-positive cells sparsely distributed in a ring-like arrangement around and on top of the eyes (e), and outlining the midbrain-hindbrain boundary (mhb). (C) In *Gt(foxd3-mcherry)*^{ct110aR} homozygotes, segmentation between the first (1) and second (2) pharyngeal arches is disrupted (white arrow). Posterior arches (3–6) are present, but show reduced sizes in homozygotes. (D) Confocal imaging shows an overall increase in mCherry-positive cells in *Gt(foxd3-mcherry)*^{ct110aR} homozygotes. Note mesenchymal-like aspect of mCherry-positive cells, with less adhesion and more cytoplasmic protrusions. In particular, large cells are widely distributed throughout the eyes and brain (arrowhead).

(E–H) Morphogenesis of the jaw cartilage is disrupted in *foxd3* mutants. Alcian Blue staining of *Gt(foxd3-mcherry)*^{ct110aR} embryos at 5 dpf. (E,G) Lateral view, anterior to the left. (F,H) Ventral views. (E,F) Craniofacial cartilage develops normally in *Gt(foxd3-mcherry)*^{ct110aR} homozygotes. (G) Cartilage defects in *Gt(foxd3m-mcherry)*^{ct110aR} homozygotes are characterized by ventral projection of the Meckel's cartilage (m) and ethmoid plate (eth). Derivatives of the second arch (ceratohyal, ch and hyosymplectic, h), as well as ceratobranchials I–V (cb i-v), are hypoplastic and malformed.

(I–J) Formation of DRGs is disrupted in *Gt(foxd3-mcherry)*^{ct110a} homozygous embryos. (I,K) Confocal projection of mCherry-positive cells in the trunk of live *Gt(foxd3-mcherry)*^{ct110a} embryos at 56 hpf. DRGs emerge from the neural tube at the level of the

anterior half of each somite. (I) FoxD3 is expressed in the glial cells associated with the DRGs (white arrows). (J) *Gt(foxd3-mcherry)*^{ct110a} homozygotes consistently lack DRGs and associated glia (white asterisks), disrupting the periodicity of DRG emergence from the neural tube.

(K–N) Specification of melanophores is delayed in FoxD3 mutants. Live embryos at 30 hpf, anterior to the left. (K,M) Lateral views. (L,N) Dorsal views. (K,L) Melanophores concentrate posterior to the otic vesicle (ov), from where they migrate over the yolk. (M,N) Melanophores are consistenly reduced in *Gt(foxd3-mcherry)*^{ct110a} homozygotes at 30 hpf. (K′,M′) Higher magnification of the boxed area.

(O–S) FoxD3 is a repressor of the melanocytic lineage at the expense of iridophore cells. (O,Q) Dorsal view of live embryos, anterior to the left. (P,R) Left lateral view, trunk region. (O) Melanophores are distributed in a characteristic pattern in the zebrafish embryo at 56 hpf. They can be individually visualized along the dorsal part of the trunk and tail (black arrowheads). (P,P′) Melanophores are also distributed as flat cells along the lateral line, mostly at the level of the trunk. (Q) In *Gt(foxd3-mcherry)*^{ct110a} homozygotes, dorsal melanophores are increased in the trunk, but not in the head region. (R) Melanophores in the lateral line are increased in homozygotes (n=14), with greater incidence of cells in the tail region (black asterisks). Melanophores appear dislocated from the lateral line and present increased cytoplasmic protrusions (R′). (S) Quantification of melanophores in the trunk and tail region of embryos at 56hpf. Significant increase was observed in homozygotes. **P<0.001. (T) Quantification of ridophores in the dorsal trunk of embryos at 52hpf. Iridophores are significantly reduced in homozygous *Gt(foxd3-mcherry)*^{ct110a} at 52 hpf. **P<0.0001. Scale bars: 50 μm.